

From laser fusion to laser accelerators: basic studies into high power laser plasmas

J Meyer-ter-Vehn

Max Planck Institute for Quantum Optics, D-85748 Garching, Germany

E-mail: meyer-ter-vehn@mpq.mpg.de

Received 17 June 2009, in final form 8 July 2009

Published 10 November 2009

Online at stacks.iop.org/PPCF/51/124001

Abstract

High power laser beams are unique in concentrating energy both in space and time. They can convert dense matter into plasma of extreme energy density. Here I shall focus on two outstanding applications. *Laser fusion* relies on isentropic compression of nuclear fuel by convergent hydrodynamic flow, and I discuss the gas dynamics underlying ignition. *Laser accelerators* depend on relativistic laser plasma interaction, generating non-neutral plasmas and accelerating fields in the range of TV m^{-1} . Self-organizing plasma structures such as channels and bubbles drive intense particle beams. Such beams may allow for fast ignition of inertial confinement fusion.

(Some figures in this article are in colour only in the electronic version)

1. Introduction

High power laser beams are unique in concentrating energy both in space and in time. The limits are set to a few micrometers by the laser wavelength and to a few femtoseconds by the light period. Thanks to the ultra-short duration, extreme powers can be achieved up to petawatts (10^{15} W) and beyond. Focused intensities are so high that target material is ionized almost instantaneously, forming dense plasmas of extremely high energy density and pressure. These plasmas allow for new applications. In this paper, I shall focus on laser fusion and laser accelerators.

Research on inertial confinement fusion (ICF) triggered by laser impact (laser fusion) is presently reaching a critical phase. At Livermore (USA), the National Ignition Facility (NIF) [1] has just been completed. A similar laser facility, the Laser MegaJoule [2], will become operational in France. Laser projects at Osaka (Japan), at Rochester (USA) and also the European project on a High Power laser Energy Research facility (HiPER) [3] aim for inertial fusion based on fast ignition. At Livermore, MJ laser pulses are expected to ignite small fuel capsules within the next two years (2010–2012). When successful, this will demonstrate self-sustained nuclear burn under controlled laboratory conditions. In these first experiments,

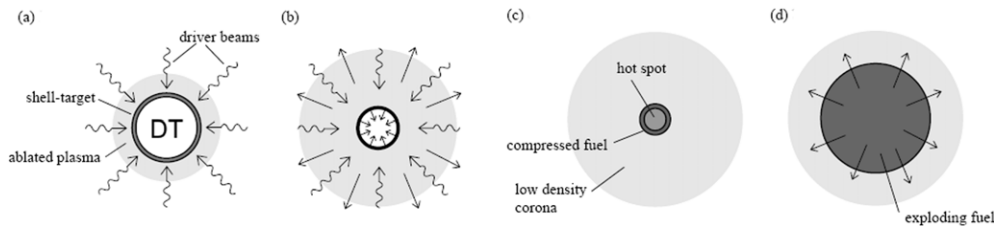


Figure 1. Principle of ICF: (a) capsule irradiation, (b) implosion driven by ablation, (c) central ignition and (d) burn and explosion.

energy gain factors of 10–20 are envisioned. This corresponds to a release of about 10^{19} fusion neutrons in a single 100 ps burst. These single-shot experiments are still far from a fusion power reactor, but they will certainly boost activities for developing inertial fusion energy (IFE).

Another new and promising branch of high power laser applications is particle acceleration. This is related to recent advances in generating laser pulses with femtosecond duration and focused intensities beyond $10^{18} \text{ W cm}^{-2}$. Many groups around the world are presently operating such lasers, and the largest project now being developed in Europe is the Extreme Light Infrastructure (ELI), aiming for exawatt (10^{18} W) pulses and focused intensities well above $10^{23} \text{ W cm}^{-2}$ [4]. At intensities beyond $10^{18} \text{ W cm}^{-2}$, relativistic laser–matter interaction sets in, and the most prominent feature is the formation of relativistic electron beams driven in the laser direction. The record result so far is a pulse consisting of 30 pC of 1 GeV electrons with an angular spread of 2 mrad [5]. Intense collimated pulses of 10–500 MeV electrons are now routinely produced. Using thin foils as targets, the primary electrons may drive intense secondary ion and photon beams. This field is developing very rapidly. Most interesting applications are expected in medicine, for both therapy and diagnostics (see e.g. [6]). Concerning inertial fusion, these relativistic beams may serve as external ignitor beams in the concept of fast ignition [7].

Over the last 20–30 years, many smaller groups have contributed to the understanding of the basic plasma physics underlying laser fusion and laser accelerators. The theoretical work covered in this paper grew out of close collaboration with the experimental laser plasma group at MPQ Garching and also with GSI Darmstadt in research on heavy ion induced inertial fusion. When I started in 1979, most details on ICF targets were still kept secret, and we had to develop our own understanding from scratch. As it turned out, some of our analytical findings helped significantly to understand the basic scalings of inertial fusion, and I shall focus on these results in the first part of this paper. The second part deals with relativistic laser–plasma interaction and the mechanisms underlying laser particle acceleration.

2. Laser fusion

2.1. Inertial confinement

The basic concept of laser fusion is illustrated in figure 1: (a) incident radiation heats a spherical capsule filled with deuterium–tritium (DT) fuel, (b) ablating plasma implodes the capsule, (c) at central stagnation the fuel ignites from a central hot spot and (d) burn propagates into the compressed fuel shell making a micro-explosion. The conditions for hot spot (labelled by h) ignition are completely set by nuclear physics. The actual values for DT fuel are

$$(\rho R)_h \approx 0.2\text{--}0.4 \text{ g cm}^{-2}, \quad T_h \approx 5\text{--}10 \text{ keV}, \quad (pR)_h \approx 15 \text{ Tbar } \mu\text{m}. \quad (1)$$

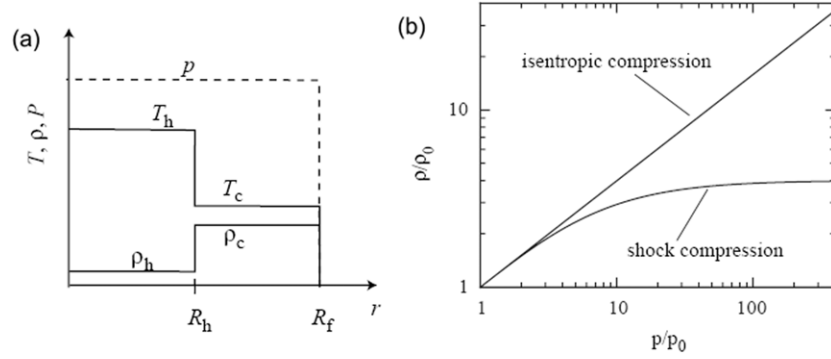


Figure 2. (a) Schematic isobaric ignition configuration consisting of a central hot spot and cold fuel outside. (b) Isentropic compression of an ideal gas along $p \sim \rho^\gamma$ compared with shock compression, having a maximum at $(\gamma + 1)/(\gamma - 1) = 4$ for adiabatic exponent $\gamma = 5/3$.

The density–radius product $(\rho R)_h$ warrants stopping of fusion α -particle inside the hot spot for self-heating, and the ignition temperature T_h ensures that self-heating just overcomes bremsstrahlung losses. Taking ideal gas pressure $p \sim \rho T$, the two conditions also set the pressure–radius product $(pR)_h$. Due to constraints (1) on ρR and pR , fuel energy and mass are proportional to inverse density and pressure squared:

$$E \sim M \sim (\rho R)^3 / \rho^2 \sim (pR)^3 / p^2. \quad (2)$$

These are the most central scaling relations for ICF. As it turns out, extreme compression is needed to keep fuel energy small enough for ignition by laser impact. Compression is also needed to reduce the fuel mass and the corresponding fusion yield to levels that can be controlled in a reactor vessel. This limits the fuel mass to a few mg.

In order to achieve high fusion gain, the hot spot needs to be surrounded by highly compressed fuel, as illustrated in figure 2(a). The fraction of fuel burnt can be estimated as $\Phi \approx \langle \rho R \rangle / (H_B + \langle \rho R \rangle)$, where $\langle \rho R \rangle = \int \rho dR$ is now the density–radius product of the fuel as a whole, and the burn parameter is $H_B \approx 6\text{--}9 \text{ g cm}^{-2}$ for the DT fuel. Apparently, one has to achieve $\langle \rho R \rangle \approx 2\text{--}3 \text{ g cm}^{-2}$ to burn 20–30% of the fuel. For a few mg of fuel, such high $\langle \rho R \rangle$ values require that the fuel is compressed by factors of 1000 and more, starting from frozen DT. In practice, this can be achieved by imploding hollow spherical shells, containing a layer of cryogenic DT on its inner surface and DT vapor in the interior.

2.2. Isentropic compression

In the early days of laser fusion research, it was not clear how such a huge compression could become feasible, mainly because fast compression involves shock waves which are known to compress matter only by a small factor. This is illustrated in figure 2(b) for a $\gamma = 5/3$ gas, for which shock compression is limited to a factor $(\gamma + 1)/(\gamma - 1) = 4$, far below 1000-fold compression. The solution to this central problem is isentropic compression according to $\rho/\rho_0 = p/p_0^{1/\gamma}$. How this can be achieved by laser-driven spherical implosion was first discussed in the open literature by Nuckolls *et al* [8]. After ten years of secret work at Livermore [9], this paper opened inertial fusion research to the academic world in 1972. The clue for high compression is to use *shaped* pressure pulses.

Though single shocks cause low compression due to excessive entropy production, a sequence of shocks following each other may lead to high compression close to adiabatic,

provided each individual shock is weak enough. Nuckolls *et al* determined the optimal power pulse numerically and found that best temporal shapes could be fitted by $P(t) \propto 1/|t_0 - t|^\beta$ with an exponent $\beta \approx 2$ [8]. Kidder then showed that $\beta = 2$ follows exactly for a $\gamma = 5/3$ gas from a model solution for homogeneous isentropic compression [10]. Actually this result can also be obtained in full generality back-on-the-envelope¹, just postulating that the radial implosion follows a power law, $R(t) \propto |t|^{-x}$ (setting $t_0 = 0$ for simplicity). Imposing conservation of mass ($M \propto \rho R^n \propto \text{const}$) and entropy ($p/\rho^\gamma \propto \text{const}$) on the implosion of a gas with adiabatic exponent γ in spherical ($n = 3$) or cylindrical ($n = 2$) geometry and using for energy $E \propto M(R/|t|)^2 \propto pR^n$ and for power $P \propto E/|t| \propto R^2/|t|^3$, one obtains

$$R(t) \propto |t|^{2/(n(\gamma-1)+2)} \propto |t|^{1/2}, \quad P(t) \propto |t|^{-(3n(\gamma-1)+2)/(n(\gamma-1)+2)} \propto |t|^{-2}, \quad (3)$$

where scalings are shown explicitly for the special case of $n = 3$ and $\gamma = 5/3$.

2.3. Fusion energy gain

Most important for applications is the prediction of energy gain $G_f = E_{\text{fus}}/E_f$, which is the ratio of fusion energy E_{fus} released and energy E_f invested into the fuel at ignition. This fuel energy is a fraction of the energy E_d deposited by the external driver, and $\eta = E_f/E_d$ is called the hydrodynamic efficiency.

Actually, the physical conditions leading to a certain energy gain can be modeled in simple terms. The typical ignition configuration is sketched in figure 2(a). At stagnation of the spherical implosion, the fuel tends to have a uniform pressure p . It then consists of a central hot spot, satisfying the ignition conditions (1), and the surrounding cold fuel. In order to achieve high gain, the energy of this highly compressed fuel reservoir has to be kept as low as possible. Actually, energy and pressure of 1000-fold compressed solid matter are close to that of degenerate electrons and are conveniently described by the entropy parameter $\alpha = p/p_F$, where $p_F(\text{Mbar}) = 2.17 (\rho_c(\text{g cm}^{-3}))^{5/3}$ is the Fermi pressure of zero temperature equimolar DT. As it turns out [11], the target energy gain

$$G = \eta G_f(E_d; p, \alpha) \quad (4)$$

can be represented as a function of the driver energy E_d just in terms of the three physical parameters:

- the overall stagnation pressure p ,
- the isentrope α of the cold compressed fuel,
- and the hydrodynamic efficiency η .

A comparison between large sets of computer simulations, obtained at the Lawrence Livermore National Laboratory (LLNL), and the model gain curves is reproduced in figure 3(a). The LLNL gain predictions represented in a *conservative* gain band could be fitted with an isentrope of $\alpha = 3$ and hydrodynamic efficiency η between 5% and 10%, while the *optimistic* gain curve corresponded to $\alpha = 1$ and $\eta = 15\%$, close to the physical limits. The model indicates a stagnation pressure of $p = 0.2 \text{ Tbar}$ and corresponds to a hot spot radius of $R_h = 75 \mu\text{m}$ according to condition (1).

The main advantage of this isobaric gain model is that it allows for scaling relations. In figure 3(b), a set of gain curves is plotted, varying the hot spot radius at fixed $\alpha = 2$ and $\eta = 10\%$. Within the model, other parameters such as fuel mass, are given implicitly, and curves of equal fuel mass are also depicted in figure 3(b). Along these curves target gain is increasing for decreasing driver energy; this is because pressure is increasing, implying smaller

¹ S Anisimov, private communication.

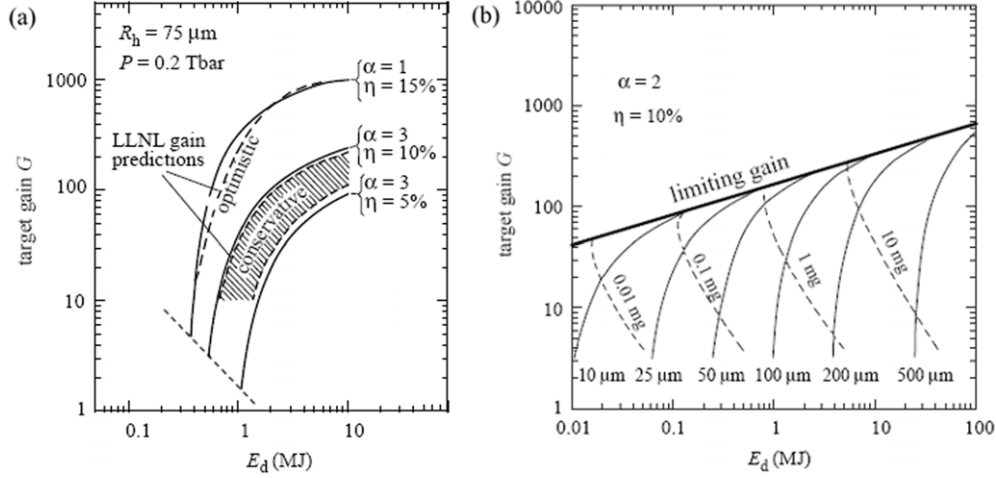


Figure 3. (a) Model gain curves compared with Livermore gain predictions [11]. (b) Sets of gain curves for fixed hot spot radius (solid), for fixed fuel mass (broken) and limiting gain. For details see text.

hot spots and decreasing ignition energy. Apparently, all these gain curves are bound from above by a limiting gain curve (thick solid line). This isobaric gain limit scales with driver energy like $G \propto E_d^{0.3}$.

2.4. Ignition energy scaling

The model given above describes gain by fuel parameters at the time of ignition. To make it more useful, these parameters need to be expressed in terms of fuel parameters during implosion, such as, e.g., implosion velocity u_{imp} . A first guess would be to equate stagnation pressure to kinetic energy density during implosion, $p \propto \rho u_{\text{imp}}^2$. Keeping entropy $\alpha \propto p/\rho^{5/3}$ fixed, this would lead to scaling of pressure and ignition energy according to

$$p \propto u_{\text{imp}}^5 / \alpha^{3/2}, \quad E_f^{\text{ign}} \propto pR^3 \propto (pR)^3 / p^2 \propto \alpha^3 / u_{\text{imp}}^{10}, \quad (5)$$

indicating an extreme dependence of ignition energy on implosion velocity. Actually, this is not confirmed by simulations. Hermann, *et al* have carried out a careful numerical study of ignition energy scaling [12]. They found that, in addition to the implosion velocity, it needs two parameters, the peak ablation pressure p_a and the in-flight isentrope parameter α_{if} , to fully characterize the dynamics of the imploding shell. Based on an extensive set of simulations, they obtained the scaling relation

$$E_f^{\text{ign}} \propto \alpha_{\text{if}}^{1.88 \pm 0.05} u_{\text{imp}}^{-5.89 \pm 0.12} p_a^{-0.77 \pm 0.03}. \quad (6)$$

One observes that, for fixed p_a and α_{if} , the energy required for ignition scales with implosion velocity as u_{imp}^6 , much weaker than the u_{imp}^{10} scaling in equation (6). As it turns out, the stagnation dynamics play a decisive role. When the compression wave of the imploding shell arrives at the center, a strong shock rebounds from the center and converts the imploding kinetic energy into thermal energy of the igniting fuel. It is this shock which increases the fuel entropy from α_{if} to α , and this affects the energy scaling significantly. In the following, we study this transformation in terms of similarity solutions, almost analytically.

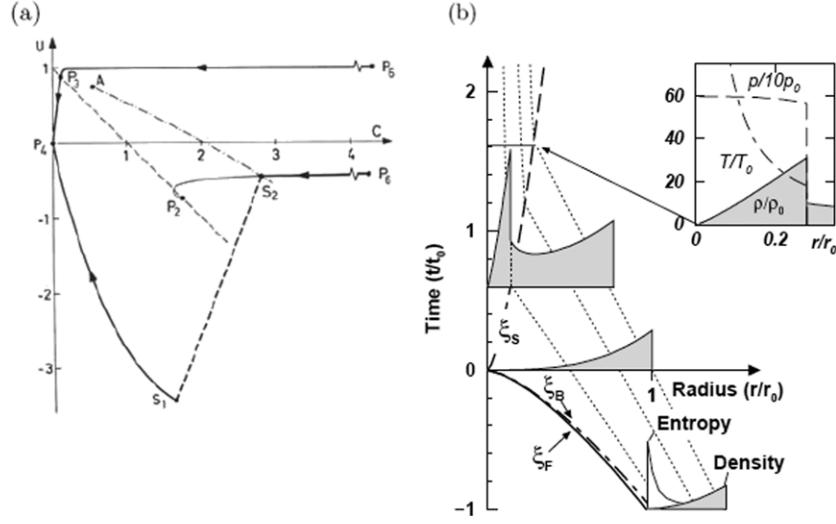


Figure 4. Similarity solution describing the implosion of a hollow shell. (a) Solution in the U, C plane for $n = 3, \gamma = 5/3, \alpha_s = 0.7, \kappa = 3$. (b) Solution in the r, t plane, showing trajectories of fluid elements (thin solid), of inner front and rebounding shock (thick solid), and profiles of density, temperature and pressure as insets.

2.5. Gas dynamics of spherical implosion

The key reference is the 1942 paper by Guderley on spherically converging shock waves [13]. Guderley discovered that, due to symmetries, the equations of gas dynamics

$$\begin{aligned} \partial\rho/\partial t + u\partial\rho/\partial r + \rho\partial u/\partial r + (n-1)\rho u/r &= 0, \\ \partial u/\partial t + u\partial u/\partial r + c^2/(\gamma\rho)\partial\rho/\partial r + (2c/\gamma)\partial c/\partial r &= 0, \\ (\partial/\partial t + u\partial/\partial r)(c^2/\rho^{\gamma-1}) &= 0, \end{aligned} \quad (7)$$

allow for similarity solutions, representing velocity $u(r, t) = \alpha_s r/t U(\xi)$, sound velocity $c(r, t) = \alpha_s r/t C(\xi)$ and density $\rho(r, t) = \rho_0 r_s^\kappa G(\xi)$ in terms of functions $U(\xi), C(\xi), G(\xi)$ of the similarity coordinate ξ . It combines radius r and time t in the form

$$\xi = r/|t|^{\alpha_s}. \quad (8)$$

The similarity ansatz contains two free parameters α_s and κ . Inserted into equations in (7), it reduces the partial differential equations to a single ordinary differential equation $dU/dC = \Delta_1(U, C)/\Delta_2(U, C)$, involving the reduced functions U and C only. Solutions of the form $U(C)$ are then connected to ξ by integrating $d \ln(\xi)/dC = \Delta(U, C)/\Delta_2(U, C)$ and $G(\xi)$ is obtained from a simple algebraic relation $G = G(U, C)$. The functions $\Delta(U, C), \Delta_1(U, C)$ and $\Delta_2(u, C)$ are simple polynomials in U and C . Explicit expressions and all other details are found in the book of Atzeni and Meyer-ter-Vehn [14].

Guderley gave a general overview of solutions in the U, C plane, and then found a particular one, corresponding to a spherical shock wave imploding in a uniform gas. Here we show a closely related solution in figure 4. It describes an imploding hollow shell. The inner front arrives at the center at time $t = 0$ (void closure), and then a strong rebounding shock emerges from the center, connecting the stagnated gas inside with the still imploding gas outside for times $t > 0$. A first important observation now is that the Mach number, $M_0 = u(r, t = 0)/c(r, t = 0) = \text{const}$, is uniform over the imploding shell at void closure.

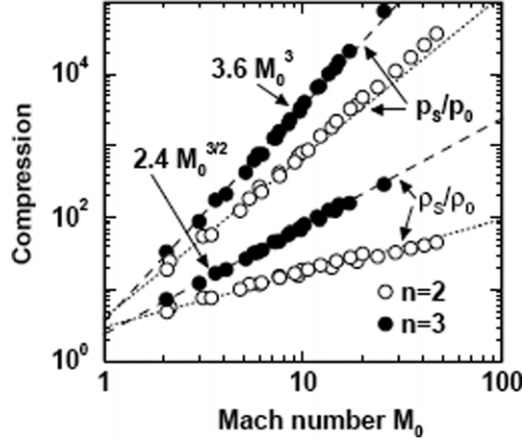


Figure 5. Compression ratios between fuel at void closure and fuel behind the rebounding shock as a function of implosion Mach number M_0 for $\gamma = 5/3$. Results for pressure and density ratios are shown both for spherical ($n = 3$, full dots) and cylindrical ($n = 2$, open dots) geometries. The dashed lines represent power law fits.

The same is true for the pressure $p(r, t = 0) \simeq p_0$ which can be identified with the peak ablation pressure $p_a \simeq p_0$, driving the shell at the outer surface. The second is that also the pressure behind the shock is uniform and can be identified with the stagnation pressure p_s . The ratio p_s/p_0 now turns out to depend almost exclusively on M_0 and very little on details of density and entropy distribution over the shell. This is found both from numerical integration [15] and from analytic treatment, which is possible for the special combination $\kappa = 2(1/\alpha - 1)$ of the free parameters [16]. The result is plotted in figure 5. One finds the important scaling relation

$$p_s/p_0 \propto M_0^{2(n+1)/(\gamma+1)} \propto M_0^3 \quad (\text{for } n = 3, \gamma = 5/3). \quad (9)$$

This relation is an approximate one, applying to spherical ($n = 3$) and cylindrical ($n = 2$) geometries and adiabatic exponents $1 < \gamma < (n + 1)/(n - 1)$. The Mach number is given by $M_0 = u_0/c_0$, where u_0 and c_0 are velocity and sound velocity at the outer boundary of the shell at $t = 0$. We now approximately identify $u_0 \simeq u_{\text{imp}}$ with the peak implosion velocity and $p_0 \simeq p_a$ with the peak drive pressure. Using $c_0 \propto (p_0/\rho_0)^{1/2}$ and $\alpha_{\text{if}} \propto p_0/\rho_0^\gamma$, we find $c_0 \propto p_a^{1/5} \alpha_{\text{if}}^{3/10}$ for a $\gamma = 5/3$ gas. This leads to the scaling relation

$$p_s \propto u_{\text{imp}}^3 p_a^{2/5} \alpha_{\text{if}}^{-9/10}. \quad (10)$$

It expresses the stagnation pressure in terms of three parameters: (1) implosion velocity u_{imp} , (2) ablation pressure p_a and (3) in-flight isentrope parameter α_{if} , which describe the imploding shell. Making use of the $E \propto p^{-2}$ scaling of equation (2), this gives the ignition energy scaling

$$E_d^{\text{ign}} = E_f/\eta \propto \eta^{-1} p_s^{-2} \propto \eta^{-1} \alpha_{\text{if}}^{1.8} u_{\text{imp}}^{-6} p_a^{-0.8} \quad (11)$$

in best agreement with the numerical results of Herrmann *et al* in equation (6). The intriguing agreement came as a surprise, because density and entropy distributions of realistic ICF capsule implosions are strongly modified by many effects, not accounted for here. Their evolution is far from self-similar. What the results seem to say is that the stagnation pressure is not sensitive to these details, but rather depends on the implosion Mach number as a global parameter. Relations (10) and (11) represent a major analytical insight into the physics of ICF implosions, found through self-similar analysis.

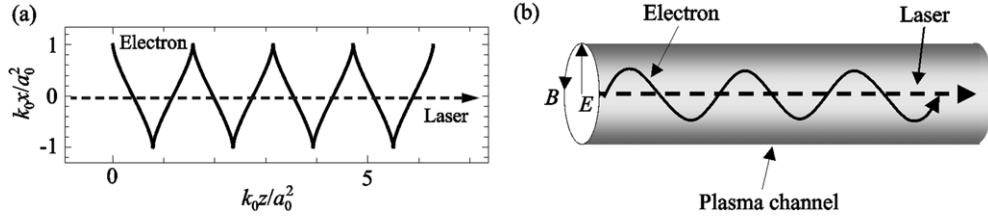


Figure 6. (a) Trajectory of single electron in vacuum driven by linear polarized light wave. (b) Electron co-moving with laser wave in a plasma channel with radial E -field and azimuthal B -field.

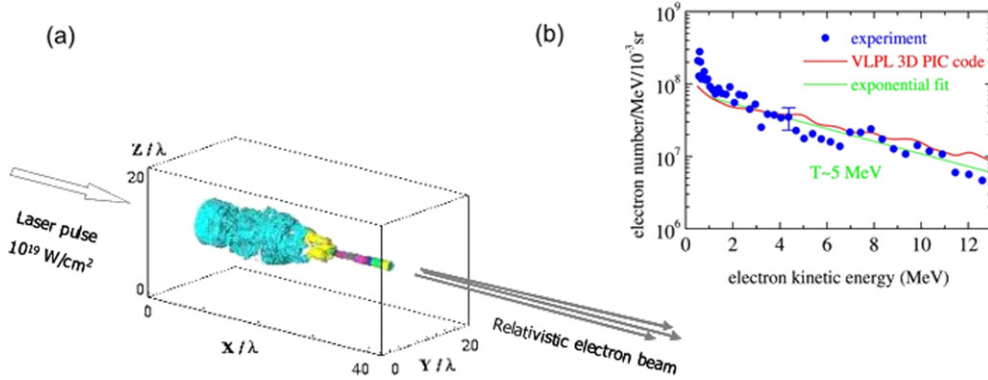


Figure 7. (a) Self-focusing of a laser beam in dense plasma (3D-PIC simulation) and electron beam accelerated in the plasma channel (schematic); (b) the corresponding electron spectrum. (Color online.)

3. Laser particle acceleration

Laser particle acceleration is another new application of high power lasers, as promising and important as laser fusion. Recent advances in laser technology [17] allow for the generation of intense pulses of femtosecond duration, using rather compact laser devices. With focused intensities above $10^{18} \text{ W cm}^{-2}$, these pulses drive target electrons to the velocity of light, and new phenomena are observed due to relativistic interaction. The most prominent feature is the generation of intense, highly directed electron beams; also secondary ion and photon beams are produced, driven by the primary relativistic electrons.

3.1. Relativistic laser plasma interaction

Expressing the laser field in terms of the normalized amplitude $a_0 = eA_0/mc^2$, the relativistic regime corresponds to $a_0 > 1$. In figure 6(a), we show the trajectory of a single electron in a strong laser field in vacuum for illustration. One observes that in addition to the transverse motion ($\sim a_0$) the electron is pushed into the laser direction ($\sim a_0^2$). This is due to the magnetic part of the Lorentz force, $(v/c) \times B_L$, which becomes as large as the electric force $\sim E_L$ for $v/c \rightarrow 1$.

In vacuum no net energy is transferred to the electron, but as soon as additional interactions come into play, electron beams are generated very efficiently. A beautiful example is given in figure 7. When focusing a laser beam with $a \simeq 3$ on a dense gas, the light beam is contracting

due to relativistic self-focusing, and an intense electron beam is emerging from the plasma channel. In figure 7(a), this is illustrated by a simulation [18]. The corresponding measured spectrum is shown in figure 7(b) [19]. An exponential energy spectrum is found, ranging up to 20 MeV and having an effective temperature of $T_{\text{eff}} \approx 5 \text{ MeV}$. The self-focusing is due to light-induced changes in the plasma frequency $\omega_p = \sqrt{4\pi e^2 n_e / m}$, both via relativistic increase in electron mass m and ponderomotive depletion of electron density n_e . The plasma channel is sketched in figure 6(b), showing the laser beam and laser-driven relativistic electrons. They are oscillating in the self-generated channel fields (azimuthal B -field due to electron current and radial E -field due to electron depletion). This configuration of co-propagating beams of electrons and light is similar to a free electron laser, known for resonant energy exchange between photons and electrons. Here electrons pick up energy from the external light beam, depending on their relative phases. Due to random electron phases, the exponential energy spectrum arises.

This mechanism of *direct laser acceleration* (DLA) turned out to be the dominant one in the experiments described above. There are, however, other very important mechanisms of laser particle acceleration, involving plasma waves and wake fields. They open the path to nearly mono-energetic spectra.

3.2. Wake field acceleration and the bubble regime

In 1979, Tajima and Dawson described how to accelerate electrons in plasma waves [20]. Driven by laser pulses in under-dense plasma, these waves propagate with phase velocities v_{ph} close to velocity of light c , and electrons co-moving with the wave can be accelerated to high energies. For laser amplitudes with $a_0 > 1$, the longitudinal electric field associated with the plasma wave can be estimated by $E_{\text{pw}}/E_0 \sim a_0$. Here, the scale is set by

$$E_0 = mc\omega_p/e = 0.96\sqrt{n_e(\text{cm}^{-3})} \text{ V cm}^{-1}. \quad (12)$$

In dense plasmas, these fields can be as high as TV m^{-1} , 5–6 orders larger than in conventional accelerators, and accordingly acceleration to GeV energy can be achieved over distances of millimeters rather than hundreds of meter.

One of the problems has been proper injection of electrons into the wave buckets. As it turned out, this can be solved easily by wave breaking and trapping of background plasma electrons. Most recent experiments on laser electron acceleration use this method. Driving the wave strongly enough, a fraction of wave electrons can reach the phase velocity and is trapped. This is different from the original scheme of Tajima and Dawson, who had considered regular 1D plasma waves below the wave breaking limit.

The regime above wave breaking was first described in detail by Pukhov and Meyer-ter-Vehn [21]. They coined it the *bubble regime*. It is illustrated in figure 8 by a three-dimensional particle-in-cell (3D-PIC) simulation [22]. An ultra-short laser pulse drives a plasma wave into under-critical plasma, which breaks after the first oscillation. Downstream wave crests are almost wiped out. In the first wave bucket, however, electron density is strongly depleted, and electrons passing on the side are partially trapped near the rear vertex, where they swing back to the center after a distance of about one plasma wavelength ($\lambda_p \approx 10\text{--}15 \mu\text{m}$). The trapped electrons are then accelerated by the longitudinal electric field of the wake (1 TV m^{-1} in the present example), and the spectrum after propagation of $200 \mu\text{m}$ is seen in figure 8(b). The accelerated electron bunch corresponds to the sharp spectral peak at $70 \pm 5 \text{ MeV}$. It contains 2×10^9 electrons and about 25% of the incident laser energy. This configuration evolves essentially in three dimensions. It is a stable self-organizing plasma regime. When driven even harder, the bubble becomes practically void of electrons, and the downstream wave

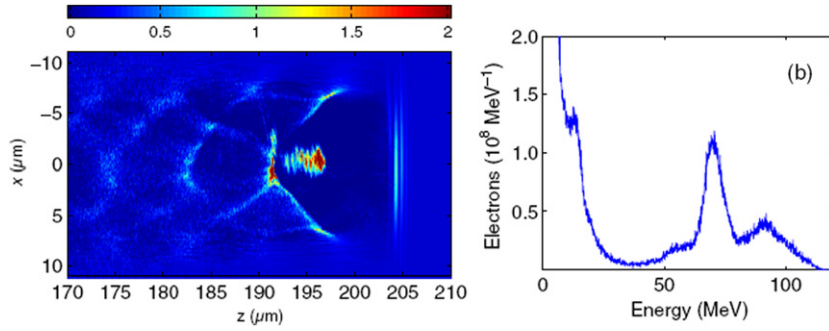


Figure 8. 3D-PIC simulation of bubble acceleration for a 5 fs, 115 mJ, $a_0 = 5$ laser pulse focused on $n_e = 1.7 \times 10^{19} \text{ cm}^{-3}$ laser plasma [22]. (a) Snapshot of plasma density when the laser pulse has propagated 205 μm into the plasma; (b) the corresponding electron spectrum. (Color online.)

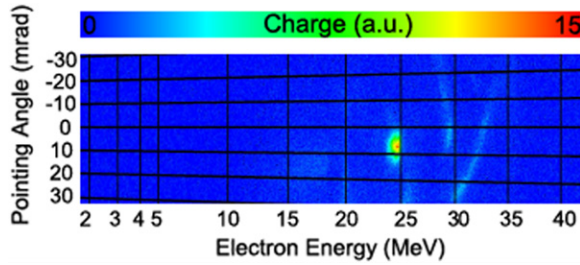


Figure 9. Electron pulse of 3 pC as observed by a magnetic spectrometer at an energy of 24.6 MeV with an energy spread of 3.3% and a divergence of 6.3 mrad. It is generated by a 8.5 fs, 20 mJ, $a_0 = 3$ laser pulse in a gas jet with a density of $n_e = 2 \times 10^{19} \text{ cm}^{-3}$ [25]. (Color online.)

structure disappears completely. The scaling of the bubble regime for $a_0 \gg 1$ was derived by Gordienko and Pukhov [23].

The quasi mono-energetic spectrum and the high efficiency of laser-to-electron energy conversion as well as the simplicity of experimental arrangements, just a single laser beam and a gas jet, make the bubble regime very attractive. An essential feature is that the laser pulse is short enough to fit into the front half of the bubble and does not overlap with the rear half in which electrons are trapped and accelerated. Such overlap leads to broad spectra, similar to DLA. In most experiments showing peaked spectra (see e.g. [24]), laser pulses were longer than the bubble, violating this condition. As it turned out, in these cases the laser pulse tends to break into pieces due to self-modulation and also compresses so that the front part finally fits into the bubble. The first experimental results using few-cycle 8.5 fs, 20 mJ, $a_0 = 3$ laser pulse that actually fits into half of the bubble [25] are given in figure 9. It shows an electron bunch resolved in energy ($24.6 \pm 0.4 \text{ MeV}$) and a divergence of 6.3 mrad, as obtained with a magnetic spectrometer. A remarkable feature is the low background in the spectrum which is attributed to the clean drive condition in this experiment. Still the energy spread is typically a few percent. Recently, Faure *et al* have demonstrated wake field acceleration with controlled electron injection by means of a second counter-propagating laser pulse [26]. This technique may prove to be the superior method to obtain more sharply peaked spectra which are required for special applications, such as laser-driven table-top XFELs [27].

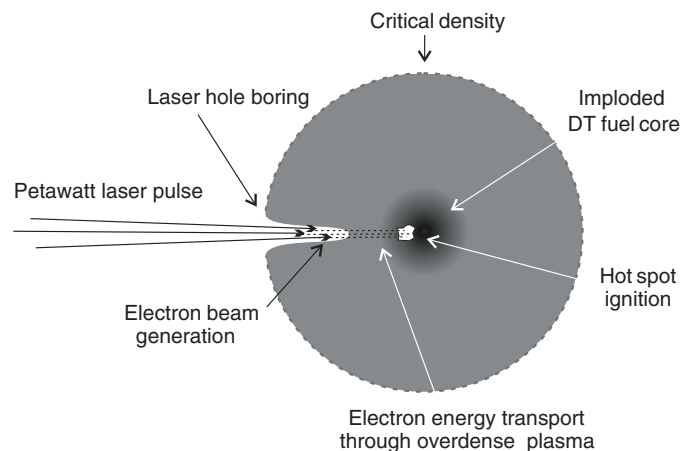


Figure 10. Scheme and physical processes of fast ignition. (Color online.)

3.3. Fast ignition

Particle acceleration with ultra-short laser pulses has also led to a promising new direction in inertial fusion research. The important point here is that the particle pulses are shorter than the time interval of inertial confinement which is typically 10–100 ps. This opens the chance for *fast ignition*, forming the hot spot for ignition by an external beam rather than by hydrodynamic convergence. Of course, this requires one to deposit 10–100 kJ in about 10 ps corresponding to multi-PW beams, but these may become feasible.

The fast ignition scheme, as first proposed by Tabak [7], is sketched in figure 10. Suppose that the fuel has been compressed to $\langle \rho R \rangle \approx 3 \text{ g cm}^{-2}$ (now without the hot spot at the center!), an external ignitor beam produces the hot spot. This beam will indent a propagation channel into the overdense fuel corona, and laser-driven electrons (or ions) have to transport the ignition energy to the core over a final distance of about 50–100 μm . The electrons should have energies of 1–2 MeV to be stopped in the dense core. Carrying PW beams involves transport of GA currents and huge magnetic fields. These currents are subject to filamentation and two-stream instability (see e.g. [28]). Simulations of fast ignition of a preformed fuel configuration, including magnetized transport through the corona and ignition physics in the compressed core, have been performed recently [29]; a representative result is shown in figure 11. It corresponds to a 50 kJ pulse of 1.6 MeV electrons and 18 ps duration injected into a model ignition configuration. It shows filamentation and self-pinching in the coronal plasma. These parameters are found to be sufficient for igniting the DT fuel.

4. Conclusions and prospects

Laser fusion and laser particle acceleration are presently developing as new fields of plasma physics with high promise for the future. Here I could touch on only a few topics. Key aspects such as hydrodynamic and kinetic instabilities, radiation transport, the structure of hot dense matter and the manifold relations to astrophysics have not been mentioned. Also the generation of ion beams and high laser harmonics from solid foils have not been discussed, although allowing for fascinating new applications in many fields of science. The high harmonics correspond to ultra-short flashes of attosecond duration, capable of resolving inner-atomic

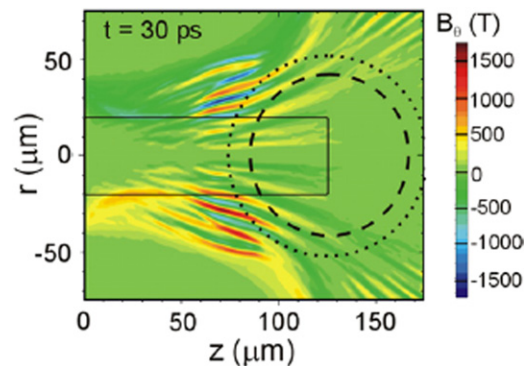


Figure 11. Fast ignition simulation [29]. It shows the magnetic field corresponding to a 50 kJ pulse of $\langle E \rangle = 1.6$ MeV electrons injected from the left-hand side. Dashed and dotted circles mark the compressed DT fuel core at 250 and 100 g cm^{-3} density. The solid line depicts the position of a perfectly collimated beam of 20 μm radius. (Color online.)

dynamics. Concerning high field physics, intensities above 10^{23} W cm^{-2} access new regimes of electromagnetic interaction, governed by radiation reaction damping, non-linear vacuum interaction and cascading electron–positron pairs. Concerning nuclear fusion, fast ignition may open new horizons for inertial fusion, igniting non-spherical configurations of compressed fuel and possibly non-DT fuels [30]. It all depends on further advances in laser technology. For young people, it is a great time to enter this field.

Acknowledgments

The author is deeply indebted to a number of excellent scientists who have strongly contributed to the work covered in this paper. Sergei Anisimov from the Landau Institute for Theoretical Physics in Moscow has provided the author with invaluable insight and advice, in particular concerning hydrodynamics and similarity solutions. The very fruitful cooperation with Stefano Atzeni from the University of Rome has led to a comprehensive textbook on inertial fusion, published by Oxford University Press. The work on heavy ion fusion and indirect drive targets would not have been possible without Mikhail Basko from the Institute of Theoretical and Experimental Physics in Moscow and Masakatsu Murakami from the Institute of Laser Engineering at Osaka. The particle-in-cell simulations of Alexander Pukhov, now at the University of Duesseldorf, have provided first insight into relativistic laser plasma physics. The long-standing cooperation with Javier Honrubia and Rafael Ramis from the Universidad Politecnica de Madrid laid the basis for much of the author’s numerical capabilities in radiation hydrodynamics (RR) and fast ignition (JH). The author also deeply acknowledges the cooperation with the experimental groups at MPQ Garching and at GSI Darmstadt as well as the large number of PhD students and Humboldt fellows. These people and others not mentioned created a most stimulating environment in which the author could work over the last 30 years.

References

- [1] National Ignition Facility <https://lasers.llnl.gov/>
- [2] Laser MegaJoule <http://www-lmj cea.fr/>
- [3] HiPER <http://www.hiper-laser.org/>

- [4] Extreme Light Infrastructure <http://extreme-light-infrastructure.eu/>
- [5] Leemans W P *et al* 2006 *Nature Phys.* **2** 696
- [6] MAP <http://www.munich-photonics.de/research-areas/area-d1/>
- [7] Tabak *et al* 1994 *Phys. Plasmas* **1** 1626
- [8] Nuckolls J H, Wood L, Thiessen A and Zimmermann G B 1972 *Nature* **239** 139
- [9] Kidder R E 1998 Laser fusion: the first ten years (1962–72) *High-power Laser Ablation SPIE Proceedings* vol 3343 ed C R Phipps (Bellingham, WA: SPIE) pp 10–33
- [10] Kidder R E 1974 *Nucl. Fusion* **14** 53
- [11] Meyer-ter-Vehn J 1982 *Nucl. Fusion* **22** 561
- [12] Herrmann M C, Tabak M and Lindl J 2001 *Nucl. Fusion* **41** 99
- [13] Guderley G 1942 *Luftfahrtforschung* **19** 302
- [14] Atzeni S and Meyer-ter-Vehn J 2004 *The Physics of Inertial Fusion* (Oxford: Clarendon)
- [15] Meyer-ter-Vehn J and Schalk C 1982 *Z. Naturf. a* **37** 955
- [16] Kemp A, Meyer-ter-Vehn J, Atzeni S 2001 *Phys. Rev. Lett.* **86** 3336
- [17] Mourou G A, Tajima T, Bulanov S 2006 *Rev. Mod. Phys.* **78** 309
- [18] Pukhov A and Meyer-ter-Vehn J 1996 *Phys. Rev. Lett.* **76** 3975
- [19] Gahn C *et al* 1999 *Phys. Rev. Lett.* **83** 4772
- [20] Tajima T and Dawson J 1979 *Phys. Rev. Lett.* **43** 267
- [21] Pukhov A and Meyer-ter-Vehn J 2002 *Appl. Phys. B* **74** 355
- [22] Geissler M, Schreiber J and Meyer-ter-Vehn J 2006 *New J. Phys.* **8** 186
- [23] Gordienko S and Pukhov A 2005 *Phys. Plasmas* **12** 043109
- [24] Mangles S *et al* 2004 *Nature* **431** 535
Geddes C *et al* 2004 *Nature* **431** 538
Faure J *et al* 2004 *Nature* **431** 541
- [25] Schmid K *et al* 2009 *Phys. Rev. Lett.* **102** 124801
- [26] Faure J *et al* 2006 *Nature* **444** 737
- [27] Gruener F *et al* 2007 *Appl. Phys. B* **86** 431
- [28] Honda M, Meyer-ter-Vehn J and Pukhov A 2000 *Phys. Rev. Lett.* **85** 2128
- [29] Honrubia J and Meyer-ter-Vehn J 2009 *Plasma Phys. Control. Fusion* **51** 014008
- [30] Atzeni S and Ciampi M L 1997 *Nucl. Fusion* **37** 1665